PAPER

First-principles study of bismuthene as a high energy density and excellent rate performance anode material for potassium-ion batteries

Physica Scripta

PAPER

First-principles study of bismuthene as a high energy density and excellent rate performance anode material for potassium-ion batteries

RECEIVED
6 October 2023

REVISED
22 November 2023

ACCEPTED FOR PUBLICATION
12 December 2023

PUBLISHED
21 December 2023

Wenfeng Pan[1], **Suiting Ning**[2], **Lili Chen**[3] and **Zhiquan Chen**[4]

[1] College of Basic Sciences, Zhengzhou University of Technology, Zhengzhou 450044, People's Republic of China
[2] School of Science, Hubei University of Technology, Wuhan 430068, People's Republic of China
[3] School of Physics and Electrical Engineering, Zhengzhou Normal University, Zhengzhou 450044, People's Republic of China
[4] Hubei Nuclear Solid Physics Key Laboratory, Department of Physics, Wuhan University, Wuhan 430072, People's Republic of China

E-mail: chenzq@whu.edu.cn

Keywords: bismuthene, potassium-ion batteries, first principles calculations

Abstract

Potassium-ion batteries (KIBs), with their abundance of resources, lower cost, high ion conductivity, and comparable redox potential, hold potential as an alternative to lithium-ion batteries (LIBs) for large-scale energy storage. Nonetheless, the scarcity of high-performance electrode materials remains a major obstacle in the advancement of KIBs. Here, the viability of bismuthene as an anode material for KIBs was systematically investigated using first-principles calculations. We found that bismuthene exhibits a maximum adsorption capacity of two layers of K atoms, offering a moderate theoretical capacity of 256.5 mAh g^{-1}. Additionally, the adsorption of K atoms on bismuthene leads to a notable enhancement in the electronic conductivity. Moreover, the ultralow average open circuit voltage (0.17 V) and diffusion barrier (0.02 eV) of K on bismuthene monolayer along the zigzag direction, suggesting a high energy density and outstanding rate performance of batteries. Hence, bismuthene demonstrates remarkable potential as a high-performance KIBs anode material, making it a hopeful contender in the field of energy storage.

1. Introduction

With the widespread use of batteries in consumer electronics, new energy electric vehicles and energy storage devices, the research and advancement of high-performance ion batteries have emerged as a significant focus within the field of materials [1–4]. Currently, lithium-ion batteries (LIBs) are widely used and highly prevalent in the battery market. However, the high price and the shortage of Li resources make LIBs cannot meet the growing demand of energy storage applications [5–7]. Therefore, other alternative energy storage batteries need to be developed. Researchers found that the amount of potassium (K) in the earth's crust (25,900 mg kg^{-1}) is significantly higher than that of Li (20 mg kg^{-1}) [8], and the cost of potassium-ion batteries (KIBs) is lower than that of LIBs. Furthermore, the ion conductivity of K ions is relatively high, and the standard redox potential of K (−2.94 V) is close to that of Li (−3.04 V) [9], so that KIBs have an opportunity to replace LIBs in the field of large-scale energy storage. However, since the atomic radius of K is greater compared to Li, the anode materials suitable for LIBs may not be suitable for KIBs [8, 10]. Thus, finding new anode materials is extremely critical to the development of KIBs.

Generally speaking, excellent anode materials for KIBs should possess significant storage capability, low average electrode potential, fast charge/discharge rate and good cycling stability [11, 12]. Several different anode materials were explored including graphite, non-graphite carbon, metals/alloys, metal oxides, metal sulfides/selenides, and various composite materials [13–19]. Among them two-dimensional materials have attracted increased interest as the anode materials for KIBs because of their large specific surface area, which can provide more adsorption sites for K resulting a relatively high specific capacity. In addition, the lattice changes of the

two-dimensional materials are small in the process of potassiation and depotassiation, leading to an excellent cycling performance. Moreover, the diffusion barrier of K ion in the two-dimensional materials is low, which makes the charging and discharging rate of the battery very fast. Given the aforementioned advantages, 2D materials are considered as prospective anode contenders for KIBs [20–23].

Bismuth is a layered rhombohedral crystal, which has many advantages such as long mean free path, high volumetric capacity (3800 mA h L^{-1}), non-toxicity and environmental friendliness, showing a certain prospect in the field of battery anode materials [24–26]. Unfortunately, the volume of bismuth changes greatly during the ion intercalation process, and the capacity decays rapidly [27, 28]. Compared with bismuth, the two-dimensional material bismuthene has a larger specific surface area and may not limit its expansion along a direction orthogonal to the surface during the ion intercalation process, thereby obtaining a better cyclic stability [27]. Shen *et al* [24] have studied few layered bismuthene nanosheets as anode materials for KIBs through experiments, and found that the few layered bismuthene nanosheets exhibits a potential in the domain of KIBs anode materials. However, the mechanisms underlying their novel performance are still not systematically explored. Therefore, this work studied the K atoms adsorption properties, storage capacity, diffusion energy barrier and average open circuit voltage using first-principles calculations to provide a theoretical reference for further experimental exploration.

2. Computational methods

First-principles calculations were performed through the Vienna *ab initio* simulation package (VASP) [29–31]. The interaction between ion cores and valance electrons was described using the projected augmented wave (PAW) method [32, 33]. The generalized gradient approximation (GGA) of Perdew–Burke–Ernzerhof (PBE) functional was employed to depict the exchange correlation potential [34]. During the calculation process, a $4 \times 4 \times 1$ supercell (32 Bi atoms) of bismuthene was employed, and the optimized lattice constant of bismuthene was 4.34 Å, corresponding to the previous studies. The k-points of the Brillouin-zone were set to $3 \times 3 \times 1$ and $5 \times 5 \times 1$ Monkhorst–Pack grid points during the process of optimizing the structure and calculating the electronic properties, respectively. A plane-wave cutoff energy of 500 eV was selected for this study. Convergence criterion was adjusted to 10^{-5} eV for energy and 0.02 eV $Å^{-1}$ for force calculations. To prevent interlayer interactions, a vacuum layer with a thickness of 20 Å was introduced orthogonal to the surface of bismuthene, and the van der Waals interaction was characterized using Grimme's DFT-D3 method [35]. The diffusion barrier of K atoms on bismuthene was calculated using the climbing image nudged elastic band (CI-NEB) method [36, 37], and the charge transfer between K atoms and bismuthene was analyzed using Bader charge [38] and the charge density difference (CDD). *Ab initio* molecular dynamics (AIMD) simulations were performed within the NVE ensemble with a time step of 2 fs, and a total time of 5 ps to evaluate the thermal stability.

3. Results and discussion

3.1. Adsorption of K on bismuthene

To explore the adsorption behavior of K atoms on bismuthene, four typical adsorption sites of K atoms on bismuthene are considered (figure 1), which are (a) above the center of the hexagonal rings (H site), (b) above the center of Bi-Bi bonds (B site), (c) above the lower Bi atoms (V site), (d) above the upper Bi atoms (T site). Moreover, the stability of K atoms adsorption at these sites was evaluated by analyzing the adsorption energy (E_{ad}), which was defined as follows:

$$E_{ad} = (E_{K+sub} - E_{sub} - nE_K)/n \quad (1)$$

Where E_{K+sub} and E_{sub} denote the energy of the bismuthene with and without K adsorption, respectively, E_K represents the energy of a K atom in its bulk metal, and n refers to the number of adsorbed K atoms. By definition, when the adsorption energy is negative, it means that the system will release heat during the adsorption process, and a more negative adsorption energy value corresponds to a more stable structure after adsorption. The studies of a single K atom at different adsorption sites show that the B and T site are not stable as they would shift to the V site after structural optimization. The adsorption energies of K at H (−0.29 eV) and V (−0.30 eV) sites are negative and similar, so H and V sites are the possible adsorption sites of K atoms on bismuthene.

Figures 2 (a)and (b) depict the adsorption structure of K atom on the V and H sites of bismuthene. Observably, the interaction between the K atom and bismuthene induces a slight deformation in the structure of bismuthene. To intuitively observe the charge transfer of K atoms and bismuthene, the charge density difference (CDD) calculation is performed, defined as:

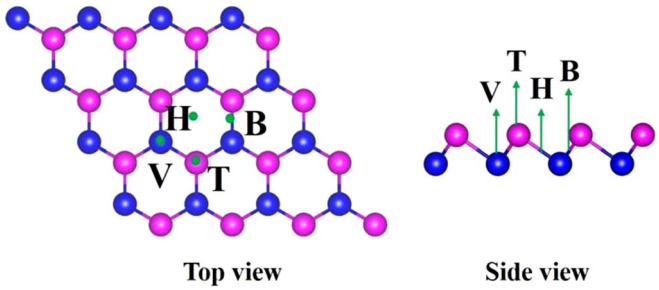

Figure 1. The top and side views of bismuthene and the typical adsorption sites of K atoms, where the fuchsia and blue spheres represent Bi atoms in the upper and lower layers, respectively.

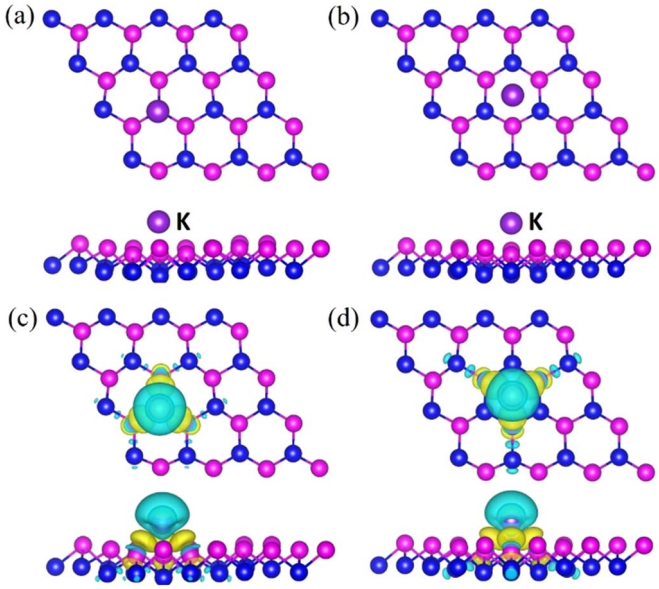

Figure 2. (a) and (b) present the adsorption structure of K atom at V and H sites, showing both top and side views, with purple spheres representing the potassium atoms. (c) and (d) are the corresponding CDD plots at V and H sites (the isosurface value is 0.0008 e/bohr^3). The yellow and blue shading represent charge gathering and charge loss respectively.

$$\Delta\rho = \rho_{K+sub} - \rho_{sub} - \rho_{k} \tag{2}$$

Where ρ_{sub} and ρ_{K+sub} represent the charge density of pristine bismuthene and K atom on bismuthene, respectively. ρ_{k} is the charge density of K. From the CDD result shown in figures 2(c) and (d), we find that the charge depletion occurs at K atom while the charge accumulation appears around the three nearby Bi atoms. This observation aligns with the result of Bader charge analysis, which indicates a transfer of 0.79 e and 0.78 e from the K atom to bismuthene at V and H sites, respectively. In addition, the large amount of charge transfer between K atom and bismuthene makes the interaction between K atom and bismuthene stronger.

The total density of states (DOS) for pristine and a single K atom adsorbed bismuthene are shown in figure 3. It is noted that pristine bismuthene possesses semiconductor characteristics, exhibiting a band gap of 0.55 eV. When a single K atom is adsorbed on bismuthene at V or H site, the Fermi level shifts towards the conduction band, resulting in enhanced electrical conductivity of bismuthene, which is crucial for the application of bismuthene in the anode material of KIBs. In addition, the partial density of states (PDOS) of bismuthene adsorbing a K atom at V and H sites reveal that the p orbital of Bi atom overlaps with both the s and p orbitals of K atom in the energy range of 0∼2.5 eV. This observation indicates a pronounced interaction between K atom and bismuthene, which makes the structures of the single K atom adsorbed bismuthene at V and H sites are stable.

The potential energy of a single K atom at different perpendicular heights (h) from the surface of bismuthene monolayer was obtained and presented in figure 4. It is clear that the potential energy of K atom at both V and H sites decreases first and then increases with the perpendicular height, and finally approaches zero. When the perpendicular height reaches approximately 2.5 Å, the lowest potential energy for the K atom is observed. As the

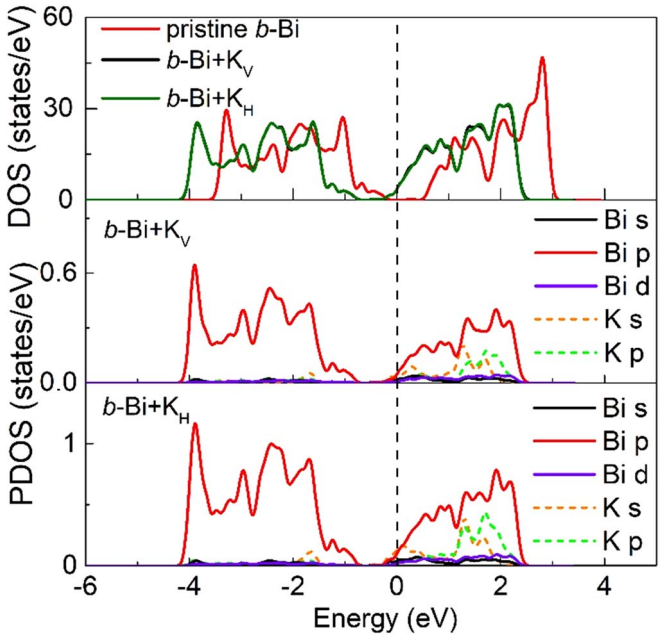

Figure 3. DOS of pristine bismuthene (pristine *b*-Bi), DOS and PDOS of bismuthene adsorbing a K atom at V site (*b*-Bi + K_V) and H site (*b*-Bi + K_H). The Fermi level is represented by black dotted line and set to zero.

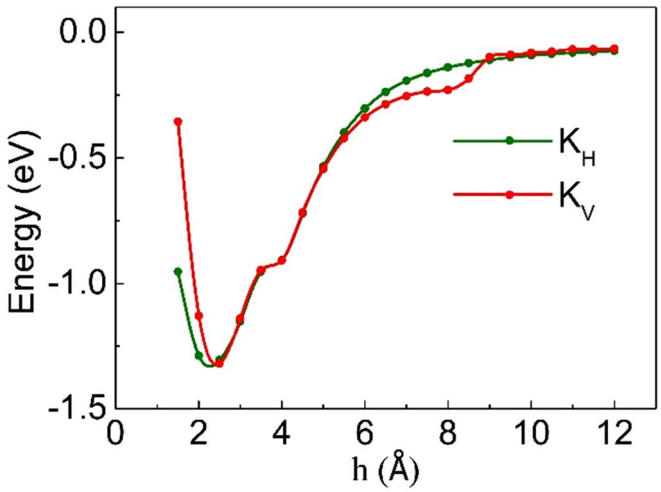

Figure 4. The change of potential energy with respect to the perpendicular height (h) of K atom on V and H sites from the bismuthene monolayer surface.

perpendicular height surpasses 8 Å, the potential energy gradually rises until it reaches zero. In this case, there is no interaction between K atom and bismuthene, and K atom can be regarded as an isolated atom. When the perpendicular height is less than 6 Å, the potential energy is significantly enhanced, indicating an intense interaction between K atoms and bismuthene. Therefore, K atoms exhibit stable adsorption on bismuthene monolayer when their perpendicular height is less than 6 Å.

3.2. Average adsorption energy and theoretical capacity

To investigate the storage capacity of bismuthene as an anode material for KIBs, the optimized adsorption configurations of multiple K atoms on bismuthene are studied shown in figure 5. The structures with chemometrics of $K_{0.03}Bi$, $K_{0.125}Bi$, $K_{0.5}Bi$, KBi, $K_{1.5}Bi$ and K_2Bi correspond to the configurations of bismuthene with 1, 4, 16, 32, 48 and 64 K atoms adsorption, respectively. For the first and second layer of K atoms adsorption, the most robust adsorption sites are calculated to be V sites and the top of T site, respectively. As illustrated in figure 5, bismuthene exhibits the ability to adsorb K atoms on both of its surfaces, with a maximum

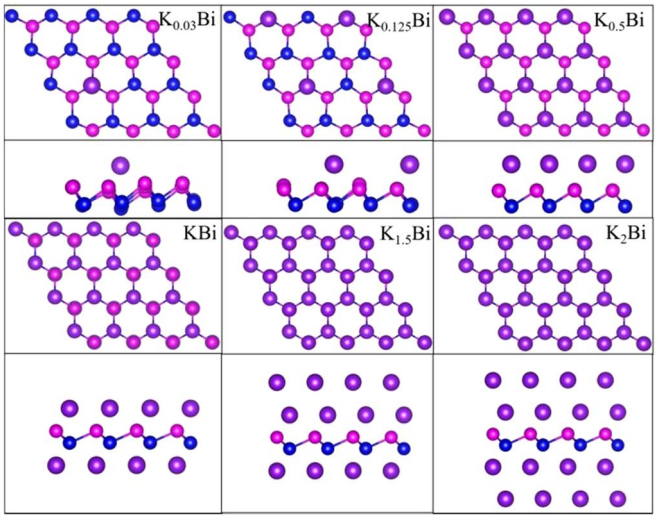

Figure 5. Top and side views of K-adsorbed bismuthene with different K concentrations.

capacity of 32 K atoms on each side. Additionally, with an increasing quantity of K atoms, the bismuthene structure has no obvious distortion, and the K atoms exhibit regular adsorption patterns on each side of bismuthene.

To investigate the stability of multilayer K atoms adsorption system, the average adsorption energy for each layer is calculated, which is specifically defined as follows:

$$E_{ave} = [E_{K_{32n}Bi} - E_{K_{32(n-1)}Bi} - 32E_K]/32 \quad (3)$$

where $E_{K_{32n}Bi}$ and $E_{K_{32(n-1)}Bi}$ are the energy of bismuthene with n and $n-1$ layers of K adsorption, respectively, and E_K is the energy of a K atom in its bulk metal. The calculated average adsorption energies for K atoms on the first and second layers are negative with the value of −0.30 and −0.06 eV, respectively. Although the average adsorption energy of K atoms on the second layer is relatively weak, it is still stronger than that of Li atoms on Mo_2C (−0.01 eV) [39] and K atoms on GeSe (−0.032 eV) [23], and Na atoms on MoN_2 (−0.02 eV) [40]. In addition, the perpendicular height of K atoms on the second layer is 6.13 Å, indicating the adsorbed K atoms on the second layer are stable and will not form metal clusters. When K atoms form three adsorption layers on both sides of bismuthene, the perpendicular height of the third layer for K atoms is higher than 8 Å, suggesting that the interaction between the third layer K atoms and bismuthene is very weak and the K atoms tend to form metal clusters. Therefore, bismuthene can adsorb a maximum of two layers of K atoms, with a total count of 64 K atoms.

Figure 6 depicts the electron localization functions (ELF) of bismuthene with the adsorption of one (KBi) and two (K_2Bi) layers of K atoms. When a single layer of K atoms is adsorbed, the valence electrons of K atoms accumulate in the outer layer, creating a negative electron cloud. This cloud effectively shields the repulsion from positive metal ions and make the adsorption layer more stable. When two layers of K atoms are adsorbed, the negative electron cloud is weaker than that of one layer of K atoms adsorption system. While the electron localization is still observed between the K atoms in the second layer and the ELF value is less than 0.5, which confirms that no metal bond is formed in the second adsorption layer. Moreover, we carried out the AIMD simulation for K_2Bi at temperatures of 300 and 500 K, as depicted in figure 7. It is apparent that there is no significant structural damage observed and the total energy exhibits minor fluctuations at 300 K. Although higher temperatures may induce more noticeable distortions, the structural integrity of K_2Bi remains preserved, with no evidence of clustering at 500 K. These finding suggest that the adsorption of K atoms on the second layer remains stable.

Based on the aforementioned discussion, we can evaluate the theoretical capacity of bismuthene using the subsequent definition:

$$C = X_{max} F/M \quad (4)$$

X_{max} is the maximum number of K atoms on bismthene, F is the Faraday constant (26.8 Ah/mol), M is the molar mass of bismuthene. Due to the large molar mass of bismuthene, the calculated theoretical capacity is 256.5 mAh g^{-1}, which surpasses that of Nb_2C (136 mAh g^{-1}) [41], YN_2 (229 mAh g^{-1}) [42], T-$NiSe_2$ (247 mAh g^{-1}) [20], GSNS (256 mAh g^{-1}) [11],but lower than the theoretical capacity of MoS_2 (335 mAh g^{-1}) [43], β-Sb (440 mAh g^{-1}) [44], C_6BN(553 mAh g^{-1}) [45] and PC_5 (835 mAh g^{-1}) [46].

The conductivity is an important factor to determine the efficacy of anode materials. Therefore, the electronic structures for bismuthene with different concentrations of K atoms are explored. As depicted in

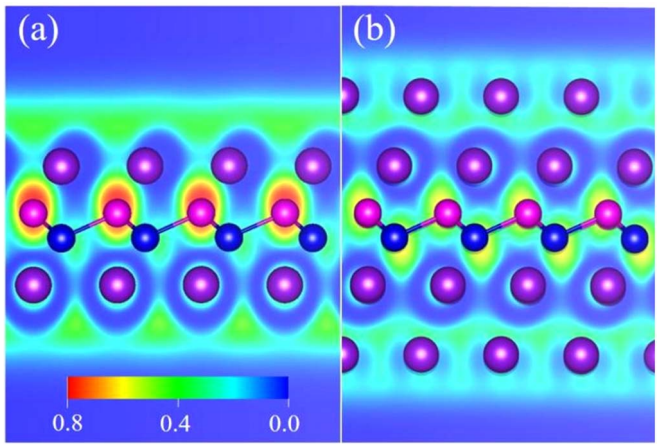

Figure 6. Electron localization function (ELF) of (100) section of (a) KBi and (b) K_2Bi. The lager ELF value indicates a higher electrons localization.

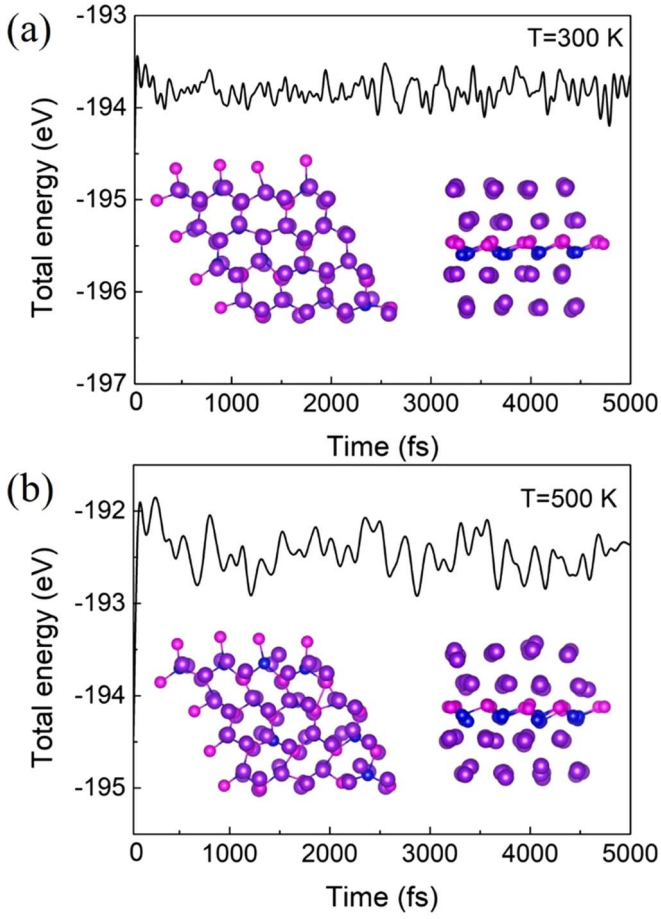

Figure 7. AIMD simulations for K_2Bi under (a) 300 K and (b) 500 K.

figure 8, the density of states of bismuthene with 4 ($K_{0.125}Bi$), 32 (KBi) and 64 (K_2Bi) K atoms adsorbed show that with the increase of K atoms, the Fermi level shifts further towards the conduction band, and eventually the band gap disappears and the system becomes metallic, similar to the phenomenon observed when K atoms are adsorbed on BP [8] and B_7N_5 [47]. What's more, the PDOS demonstrates that the electron states near the Fermi level primarily originate from the p orbitals of Bi atoms and the s and p orbitals of K atoms. In addition, the p orbitals of Bi atoms around the Fermi level are generated by the electrons transferred from the adsorbed K atoms, which improve the electrical conductivity of the system.

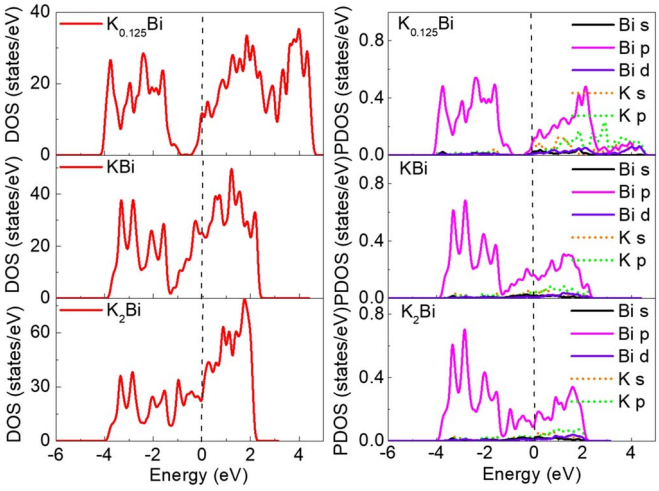

Figure 8. DOS and PDOS of $K_{0.125}Bi$, KBi and K_2Bi.

3.3. Average open circuit voltage

The average open circuit voltage (OCV) of the anode material is also an important parameter to measure its performance, which can be expressed in the following formula:

$$V_{ave} = [E_{sub} + X_{max}E_K - E_{K+sub}]/X_{max}e \quad (5)$$

where E_{sub} and E_{K+sub} are the energy of bismuthene before and after K atoms adsorption, X_{max} is the maximum number of adsorbed K atoms, and E_K is the energy of a K atom in its bulk metal, respectively. The calculated OCV value is 0.17 V, which is within the favorable potential ranges (0.1–1.0 V) for anode material [48–50], and lower than the OCV value of VN_2 (0.77 V) [51], NiB_6 (0.69 V) [52] and C_3NS (0.36 V) [53], C_3N (0.26 V) [54] for K. Therefore, bismuthene can provide a higher energy density as an anode material for KIBs.

3.4. Volume expansion

The volume expansion of anode materials during the charge/discharge process has a detrimental impact on the long-term stability of batteries. Thus, the large volume expansion of bulk bismuth during the cycle process limits its application in electrode materials. In order to analyze the cyclic stability of bismuthene, the change of lattice constant of bismuthene after K atoms adsorption was calculated using $(l\text{-}l_0)/l_0$, where l and l_0 are the lattice constants of pristine bismuthene and bismuthene adsorbed with K atoms, respectively. The maximum change in lattice constants is 13.0%, corresponding to a volume expansion of 27.7%. Compared with the large volume expansion (250%)[55] of bulk bismuth as the anode material for sodium-ion batteries, the volume expansion of bismuthene is small. Therefore, the structural stability of bismuthene in the charge/discharge process is significantly enhanced in comparison to bulk bismuth, which is beneficial for prolong the service life of KIBs.

3.5. Diffusion properties of K on bismuthene

The mobility of K is a crucial factor influencing the charge–discharge rate of KIBs. Hence, the diffusion energy barriers of the K on bismuthene are studied. Since the V site is the strongest binding site for K atoms on the surface of bismuthene monolayer, our research focuses primarily on examining the diffusion of K atoms between two adjacent V sites. Figure 9(a) presents the diffusion pathways of K atoms along the zigzag direction (Path 1: V → H → V) and the armchair direction (Path 2: V → T → V). From the diffusion energy barriers diagram in figure 9(b), it is evident that when K atoms diffuse along Path 1, they pass through two saddle points with similar barriers and there exists a local minimum between these two saddle points, which corresponds to the H site on the bismuthene surface. The obtained diffusion energy barrier for Path 1 is merely 0.02 eV, which is lower than the diffusion energy barriers of K on the surfaces of other two-dimensional materials such as C_3NS (0.24 eV) [53], PC_5 (0.18 eV) [46], C_6S (0.11 eV) [56], B_7N_5 (0.10 eV) [47], C_6BN (0.09 eV) [45], BeN_4 (0.062 eV) [21] and TNRs (0.029 eV) [57]. This suggests that K can rapidly diffuse on the bismuthene surface, making bismuthene an excellent anode material for KIBs with exceptional rate performance. The diffusion energy barrier of K along Path 2 is 0.13 eV, which is much higher than that along Path 1. This is because the diffusion of K along Path 2 passes through the T site, and the stability of T site on the surface of bismuthene is lower than that of H site, so the diffusion energy barrier for K along Path 2 is higher compared to that along Path 1.

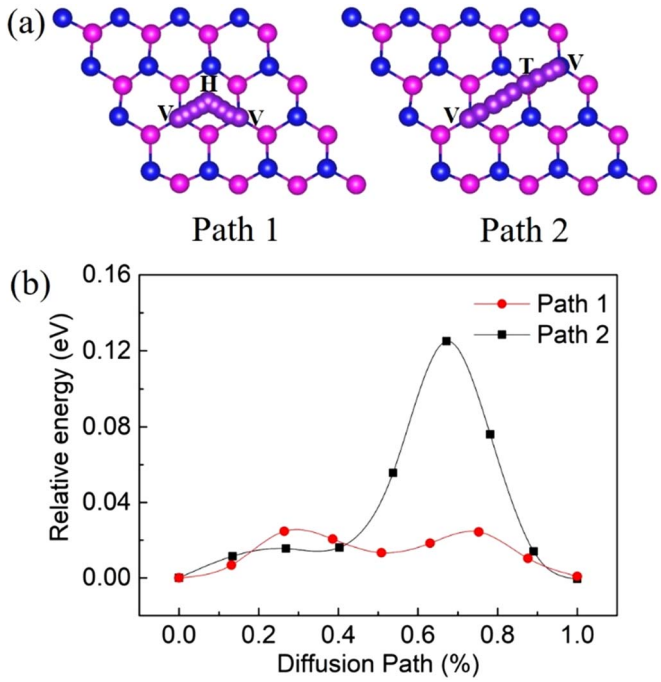

Figure 9. (a) Diffusion pathways and (b) corresponding energy barriers for K through Path 1 and Path 2 on bismuthene monolayer.

According to the Arrhenius equation, the diffusion coefficient can be calculated as follows:

$$D = a^2 \nu e^{-\frac{E_a}{k_B T}} \tag{6}$$

Where a is the diffusion distance, ν is the frequency factor and can be approximated as 10^{13} HZ, E_a represents the diffusion energy barrier, and k_B corresponds to the Boltzmann constant. When the temperature T is 300 K, the calculated diffusion coefficients of Path 1 and Path 2 are 1.54×10^{-2} and 5.73×10^{-4} $cm^2\ s^{-1}$, respectively. This demonstrates that the diffusion coefficient for K along the zigzag direction is about 26 times greater than that along the armchair direction, implying the anisotropic diffusion for K on the bismuthene.

In addition, the diffusion energy barrier of K across monolayer bismuthene (Path 3) is also calculated. As shown in figure 10, there is only one saddle point in the diffusion path of K from an H site on the upper surface to an H site on the lower surface of bismuthene, which corresponds to the K atoms being in the middle of the upper and lower layers of bismuth atoms. Due to the poor stability of the system at this saddle point, the energy barrier for K diffusion along Path 3 is very high (2.63 eV), indicating that K cannot diffuse through the bismuthene monolayer.

3.6. Comparison with bismuthene bilayer

To explore the impact of dimensionality on bismuthene's performance, we computed the adsorption behavior of K on bismuthene bilayer. Figure 11 depicts the potential adsorption sites for K atoms on bismuthene bilayer. T1, V1, H1 and B1 are the sites of K adsorbed on the outside surface of bismuthene bilayer, which are similar to site T, V, H and B on bismuthene monolayer. V2 and B2 are the sites of K embedded in the interlayer of bismuthene bilayer, which are similar to site V and B on bismuthene monolayer. Among them, the B1 site is an unstable adsorption site, with the K atoms automatically moving to the V1 site after structural optimization. This behavior is similar to the adsorption observed on the B site of bismuthene monolayer. The adsorption energies of K atoms on T1, V1, H1, V2, and B2 sites are calculated to be −0.27, −0.61, −0.62, 0.57 and 0.52 eV, respectively. Obviously, the H1 site exhibits the strongest adsorption energy, while the V2 and B2 positions display relatively weaker adsorption energies. Therefore, K atoms are more likely to be adsorbed at H1 sites on the surface of bismuthene than at interlayer sites of bismuthene. Consequently, we explored the potential energy of K atom at H1 site with different perpendicular height between the bismuthene bilayer surface (figure 12). It is clear that when the height exceeds 8 Å, the potential energy approaches zero, and the K has no interactions with bismuthene bilayer. Within 6 Å, however, the potential energy experiences a significant decrease, suggesting a robust interaction between K and the bismuthene bilayer.

To evaluate the storage capacity of bismuthene bilayer as an anode material for KIBs, we investigated the optimized adsorption configurations of multiple K atoms on bismuthene bilayer, as depicted in figure 13. The structures with chemometrics of KBi_2 and K_2Bi_2 represent bismuthene bilayer with 32 and 64 adsorbed K atoms,

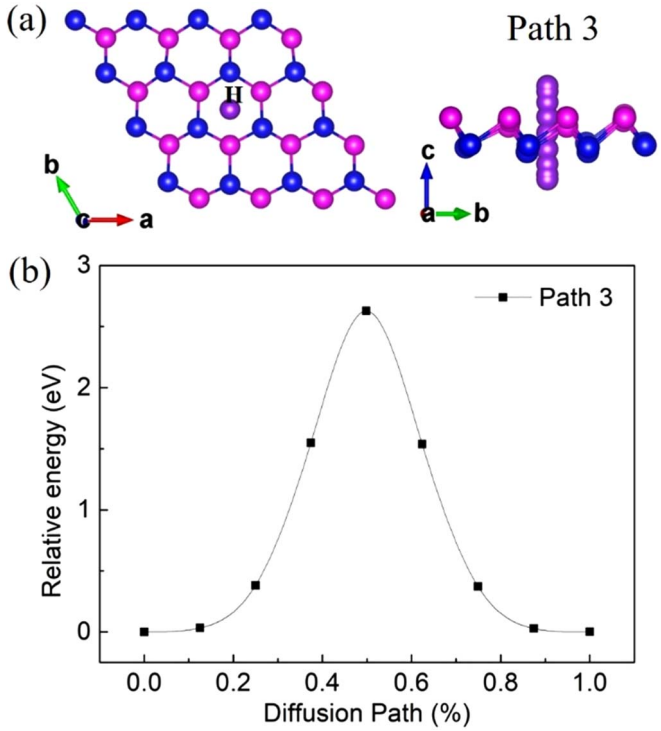

Figure 10. (a) Diffusion pathway of K across bismuthene monolayer from top and side views and (b) corresponding energy barrier.

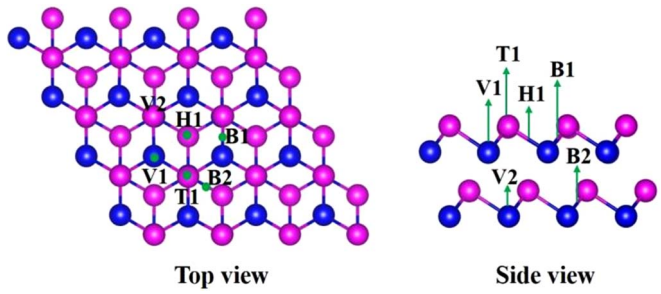

Figure 11. Potential adsorption sites for K atoms on bismuthene bilayer include top and side views.

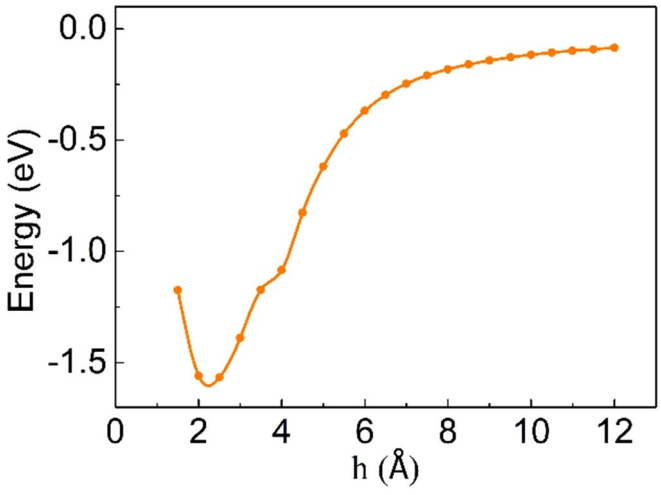

Figure 12. The change of potential energy with respect to the perpendicular height (h) of K atom from the bismuthene bilayer surface.

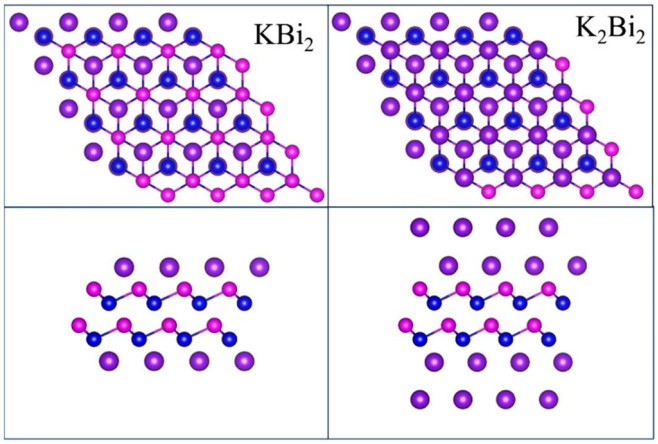

Figure 13. Top and side views of K-adsorbed bismuthene bilayer with different K concentrations.

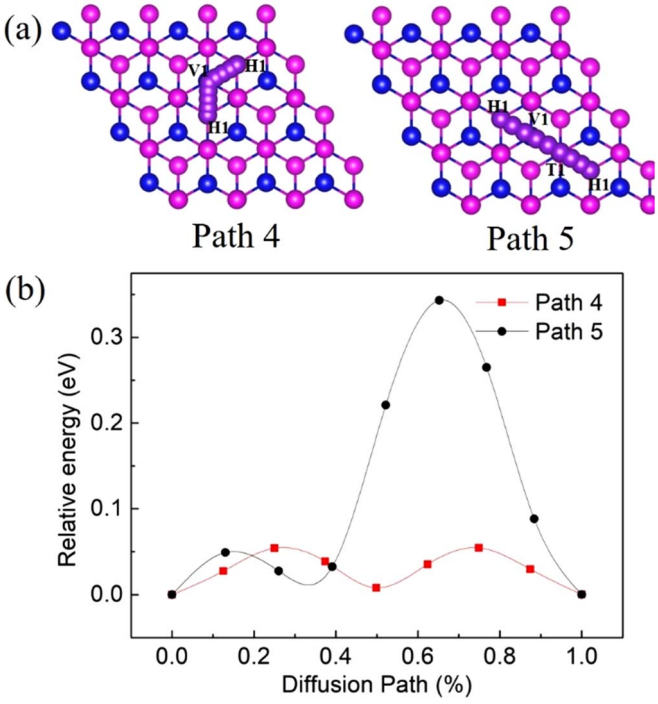

Figure 14. (a) Diffusion pathways and (b) corresponding energy barriers of K through Path 4 and Path 5 on bismuthene bilayer.

respectively. Bismuthene bilayer demonstrates an ability to adsorb K atoms on both surfaces, with a maximum capacity of 32 K atoms on each side. The average adsorption energies for K atoms on the first and second layers are −0.45 eV and −0.04 eV, respectively. Furthermore, the perpendicular height of K atoms on the second layer is 5.97 Å, suggesting their stability without forming metal clusters. However, when three layers of K atoms are adsorbed on both sides of bismuthene bilayer, the perpendicular height of the third layer (9.83 Å) exceeds 8 Å, indicating weak interaction and a tendency for K atoms to form clusters. Therefore, bismuthene bilayer can adsorb up to two layers of K atoms with a theoretical capacity of 128.3 mAh g^{-1}, which is much lower than that of bismuthene monolayer. We also calculated the OCV and Volume expansion of the bismuthene bilayer. The OCV is 0.25 V, and the maximum change in lattice constants is 8.98%, corresponding to a volume expansion of 18.8%. Obviously, the bismuthene bilayer exhibits lower energy density and higher cyclic stability compared to bismuthene monolayer.

Moreover, we explored the diffusion barriers between adjacent H1 sites on the bilayer bismuthene surface. Figure 14 shows the diffusion paths of K on the bilayer bismuthene surface along the zigzag direction (Path 4: H1 → V1 → H1) and the armchair direction (Path 5: H1 → V1 → T1 → H1). The diffusion energy barrier along the H1 → V1 → H1 path for K on bismuthene bilayer is similar to that on bismuthene monolayer along the V → H

→ V path, both exhibiting two saddle points and one local minimum. However, the diffusion energy barrier for K on the bismuthene bilayer (0.05 eV) is greater than that on the bismuthene monolayer (0.02 eV), and the diffusion coefficient of K on the bilayer bismuthene is 3.92×10^{-3} cm^2 s^{-1}, which is about one quarter of the diffusion coefficient on the monolayer bismuthene. Furthermore, the diffusion energy barrier of K on bismuthene bilayer along the H1 → V1 → T1 → H1 pathway exhibits a similar profile to that on the bismuthene monolayer along the V → T → V pathway. The diffusion energy barrier along the H1 → V1 → T1 → H1 pathway on the bismuthene bilayer is 0.34 eV, resulting in a diffusion coefficient of 1.31×10^{-7} cm^2 s^{-1}, which is significantly slower than the diffusion rate of K on the bismuthene monolayer along the V → T → V pathway. In addition, the diffusion anisotropy of K on the bismuthene bilayer is more pronounced, with the diffusion rate along the zigzag direction being 3×10^4 times higher compared to that along the armchair direction. This makes it impossible for K to diffuse along Path 5 on the bismuthene bilayer surface. In summary, the diffusion rate of K on the bismuthene monolayer is significantly higher compared to that on the bismuthene bilayer. Therefore, reducing the dimensionality of bismuthene anode material is expected to improve the rate performance of bismuthene during charge and discharge.

4. Conclusions

In summary, we have employed first-principles methods to explore the prospective utilization of bismuthene as anode material in KIBs. Our study reveals that with the adsorption of K atoms, the Fermi level shifts towards the conduction band, providing considerable electrical conductivity of bismuthene. With the increase of K atoms adsorbed on bismuthene, the average adsorption energy decreases from −0.30 eV (single layer) to −0.06 eV (double layer), and the maximum adsorption capacity of K on bismuthene monolayer surface is two layers, corresponding to a theoretical capacity of 256.5 mAh g^{-1}. Despite its modest theoretical capacity, bismuthene monolayer exhibits a low average open circuit voltage (0.17 V), relatively small lattice constant variation and very low diffusion barrier (0.02 eV), providing a high energy density, good cycling stability and outstanding rate performance for KIBs. In addition, by comparing the performance of monolayer and bilayer bismuthene, it is found that the dimensionality reduction is conducive to the storage capability, charge/discharge rate and energy density, but not benefit to the cycling stability of bismuthene as anode material for KIBs.

Data availability statement

All data that support the findings of this study are included within the article (and any supplementary files).

Acknowledgments

This work was supported by the National Natural Science Foundation of China under Grant Nos. 12175166 and 12075173, and the National Key R&D Program of China (2019YFA0210003). The calculations involved in this paper have been done on the supercomputing system in the Supercomputing Center of Wuhan University.

ORCID iDs

Wenfeng Pan https://orcid.org/0009-0009-9326-6652
Zhiquan Chen https://orcid.org/0000-0002-9518-7837

References

[1] Whittingham M S, Savinell R F and Zawodzinski T 2004 *Chem. Rev.* **104** 4243–4
[2] Wu Y, Huang L, Huang X, Guo X, Liu D, Zheng D, Zhang X, Ren R, Qu D and Chen J 2017 *Energy Environ. Sci.* **10** 1854–61
[3] Liang B, Ma N, Wang Y, Wang T and Fan J 2022 *Appl. Surf. Sci.* **599** 153927
[4] Gao N, Ye P, Chen J, Xiao J and Yang X 2023 *Langmuir* **39** 10270–9
[5] Hwang J Y, Myung S T and Sun Y K 2018 *Adv. Funct. Mater.* **28** 1802938
[6] Ji B, Zhang F, Wu N and Tang Y 2017 *Adv. Energy Mater.* **7** 1700920
[7] Liu H, Cai Y, Guo Z and Zhou J 2022 *ACS Omega* **7** 17756–64
[8] Mukherjee S, Kavalsky L and Singh C V 2018 *ACS Appl. Mater. Interfaces* **10** 8630–9
[9] Komaba S, Hasegawa T, Dahbi M and Kubota K 2015 *Electrochem. Commun.* **60** 172–5
[10] Zhou Y, Zhao M, Chen Z W, Shi X M and Jiang Q 2018 *Phys. Chem. Chem. Phys.* **20** 30290–6
[11] Li F, Qu Y and Zhao M 2016 *J. Mater. Chem. A* **4** 8905–12
[12] Zhang Z, Yang M, Zhao N, Wang L and Li Y 2019 *Phys. Chem. Chem. Phys.* **21** 23441–6
[13] Liang H-J, Gu Z-Y, Zheng X-Y, Li W-H, Zhu L-Y, Sun Z-H, Meng Y-F, Yu H-Y, Hou X-K and Wu X-L 2021 *J. Energy Chem.* **59** 589–98
[14] Sultana I, Rahman M M, Chen Y and Glushenkov A M 2018 *Adv. Funct. Mater.* **28** 1703857

[15] Liang H-J et al 2022 Sci. Bull. 67 1581–8
[16] Lin J, Lu S, Zhang Y, Zeng L, Zhang Y and Fan H 2023 J. Colloid Interf. Sci. 645 654–62
[17] Ma M, Chong S, Yao K, Liu H K, Dou S X and Huang W 2023 Matter 6 1–54
[18] Zhang K-Y, Gu Z-Y, Ang E H, Guo J-Z, Wang X-T, Wang Y and Wu X-L 2022 Mater. Today 54 189–201
[19] Min X, Xiao J, Fang M, Wang W, Zhao Y, Liu Y, Abdelkader A M, Xi K, Kumar R V and Huang Z 2021 Energy Environ. Sci. 14 2186–243
[20] Shen Y, Liu J, Li X and Wang Q 2019 ACS Appl. Mater. Interfaces 11 35661–6
[21] Cheng Z, Zhang X, Zhang H, Liu H, Yu X, Dai X, Liu G and Chen G 2023 J. Alloys Compd. 936 168351
[22] Gong S and Wang Q 2017 J. Phys. Chem. C 121 24418–24
[23] Sannyal A, Zhang Z, Gao X and Jang J 2018 Comput. Mater. Sci. 154 204–11
[24] Shen C et al 2020 J. Mater. Chem. A 8 453–60
[25] Lei K, Wang C, Liu L, Luo Y, Mu C, Li F and Chen J 2018 Angew. Chem. Int. Ed. 57 4687–91
[26] Li X, Ni J, Savilov S V and Liang L 2018 Chem. Eur. J. 24 13719–27
[27] Zhou J et al 2019 Adv. Mater. 31 1807874
[28] Sottmann J, Herrmann M, Vaj Ee Ston P, Hu Y, Ruud A, Drathen C, Emerich H, Fjellvåg H and Wragg D S 2016 Chem. Mater. 28 2750–6
[29] Kresse G and Hafner J 1993 Phys. Rev. B 47 558–61
[30] Kresse G and Hafner J 1994 Phys. Rev. B 49 14251–69
[31] Kresse G and Furthmüller J 1996 Comput. Mater. Sci. 6 15–50
[32] Kresse G and Joubert D 1999 Phys. Rev. B 59 1758–75
[33] Blöchl P E 1994 Phys. Rev. B 50 17953–79
[34] Perdew J P, Burke K and Ernzerhof M 1998 Phys. Rev. Lett. 77 3865–8
[35] Grimme S, Antony J, Ehrlich S and Krieg H 2010 J. Chem. Phys. 132 154104
[36] Henkelman G and Jónsson H 1999 J. Chem. Phys. 111 7010–22
[37] Henkelman G, Uberuaga B P and Jónsson H 2000 J. Chem. Phys. 113 9901–4
[38] Henkelman G, Arnaldsson A and Jónsson H 2006 Comput. Mater. Sci. 36 354–60
[39] Sun Q, Dai Y, Ma Y, Jing T, Wei W and Huang B 2016 J. Phys. Chem. Lett. 7 937–43
[40] Zhang X, Yu Z, Wang S, Guan S, Yang H, Yao Y and Yang S 2016 J. Mater. Chem. A 4 15224–31
[41] Hu J P, Xu B, Ouyang C Y, Zhang Y and Yang S Y A 2016 RSC Adv. 6 27467–74
[42] Gong S, Zhang C, Wang S and Qian W 2017 J. Phys. Chem. C 121 10258–64
[43] Rehman J, Fan X, Laref A, Dinh V A and Zheng W T 2021 J. Alloys Compd. 865 158782
[44] Shaikh G A, Cornil D, Gupta S K, Ahuja R and Gajjar P N 2022 Energy Fuels 36 7087–95
[45] Xiang P, Sharma S, Wang Z M, Wu J and Schwingenschlogl U 2020 ACS Appl. Mater. Interfaces 12 30731–9
[46] Lin H, Zhu L, Zhang Z, Jin R, Huang Y and Hu Y 2022 Colloid Surface A 643 128756
[47] Xiong Y, Wang Y, Ma N, Zhang Y, Luo S and Fan J 2023 Phys. Chem. Chem. Phys. 25 24303–12
[48] Xiang P, Chen X, Xiao B and Wang Z M 2019 ACS Appl. Mater. Interfaces 11 8115–25
[49] Çakır D, Sevik C, Gülseren O and Peeters F M 2016 J. Mater. Chem. A 4 6029–35
[50] Yadav N, Chakraborty B and Dhilip Kumar T J 2021 Phys. Chem. Chem. Phys. 23 11755–63
[51] Dong Y, Tang Z, Liang P, Wan H, Wang H, Wang L, Shu H and Chao D 2021 J. Colloid Interf. Sci. 593 51–8
[52] Tian B, Du W, Chen L, Guo J, Shu H, Wang Y and Dai J 2020 Appl. Surf. Sci. 527 146580
[53] Gao J, Tang M, Zhang X and Yang G 2022 J. Phys. Chem. Lett. 13 12055–60
[54] Bhauriyal P, Mahata A and Pathak B 2018 J. Phys. Chem. C 122 2481–9
[55] Sun J, Li M, Oh J, An S and Zeng K 2018 Mater. Technol. 33 563–73
[56] Tang M, Schwingenschlögl U and Yang G 2022 Mater. Today Chem. 25 100951
[57] Younis U, Muhammad I, Kawazoe Y and Sun Q 2020 Appl. Surf. Sci. 521 146456